

Micromagnetic Simulations of Magnetoresistive Behavior of Sub-Micrometer Spin-valve MRAM Devices

John O. Oti and Stephen E. Russek

Electromagnetic Technology Division, National Institute of Standards and Technology, Boulder, Colorado

Abstract—The effects of device shape and size on the giant magnetoresistive (MR) response of $\text{NiFe}_{7.5\text{nm}}/\text{Co}_{0.6\text{nm}}/\text{Cu}_{3\text{nm}}/\text{Co}_{0.6\text{nm}}/\text{NiFe}_{7.5\text{nm}}/\text{FeMn}$ spin-valve magnetoresistive random access memory (MRAM) stripes are studied by micromagnetic simulation. Samples having aspect ratios of 10:1, 3:1 and 1.5:1, and line widths varying from 0.5 μm to 1.5 μm are simulated. The effects of the magnetostatic coupling between the magnetic layers and their self-demagnetization are studied.

I. INTRODUCTION

Giant magnetoresistive (GMR) spin-valve devices are actively being investigated for use as memory elements in non-volatile solid-state magnetic random access memory (MRAM) applications [1]. Their simple structure and higher MR ratios compared to traditional anisotropic magnetoresistive (AMR) devices [2], are very desirable properties for high-speed, highly integrated MRAM applications. Other GMR devices such as spin-dependent tunneling (SDT) devices [3] also are good candidates for high performance MRAMs.

A typical MRAM spin valve is illustrated schematically in Fig. 1(a). The device consists of a sandwich structure of two magnetic layers that are separated by a nonmagnetic spacer layer. The magnetization of one of the magnetic layers (the top layer in the figure) is pinned along the long dimension of the device by an antiferromagnetic exchange-biasing overcoat layer (not shown in the figure), while the magnetization of the second layer is free to rotate. A system of current-carrying conductors connect the device to external current sources and generate a magnetic field H for operating it. This field is directed along the long dimension of the device. The conductors form part of a larger circuit that implements the read and write functions of a MRAM cell. For normal device operation, field excursions of limited magnitude are applied, so that only the magnetization of the free layer reverses completely, while that of the pinned layer remains relatively unchanged. Fig. 1(b) depicts the rectangular-shaped MR response curve of an ideal MRAM spin valve. The ideal spin valve requires a stable uniformly pinned magnetization of the pinned layer, a free magnetic layer that switches in a bi-stable manner and switching thresholds that are symmetrical about the vertical axis.

Magnetostatic effects, which are highly dependent on the geometrical properties of a device, cause its MR response to depart from the ideal response [4,5].

It is necessary to fully understand these effects in order to fabricate useful devices. In this article we describe a micromagnetic study of the dependence of the MR response of a MRAM spin valve on device shape and size, for the structure $\text{NiFe}_{7.5\text{nm}}/\text{Co}_{0.6\text{nm}}/\text{Cu}_{3\text{nm}}/\text{Co}_{0.6\text{nm}}/\text{NiFe}_{7.5\text{nm}}$. The thin layer of Co between the NiFe and Cu layers enhances the MR response of the spin valves [6]. Samples having aspect ratios of 10:1, 3:1 and 1.5:1, and line widths varying from 0.5 μm to 1.5 μm are simulated using both whole and fractional bulk magnetization values. The fractional values are intended to simulate possible magnetization reduction due to interface effects or degradation of the sample during device processing.

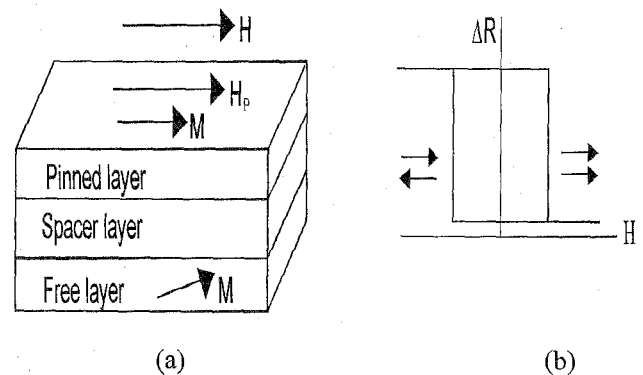


Fig. 1. MRAM spin valve: (a) Schematic of sandwich structure. (b) MR curve of ideal MRAM spin valve. The arrow pairs in the MR plot illustrate the relative orientations of the magnetization vectors of the pinned (top arrow) and free layers at the different parts of the curve.

II. SIMULATION

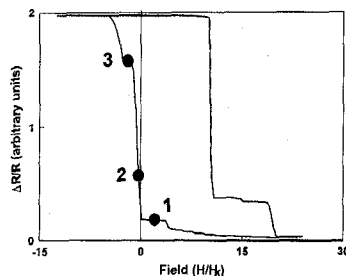
The simulations presented below were carried out using a dual-layer micromagnetic model [7] in which each magnetic layer is modeled by a monolayer of discrete parallelepiped elements having square cross sections in the film plane. The elements represent the grains of the layers. Each grain has a fixed magnitude magnetic moment which is allowed to dynamically relax (in three dimensions) in the presence of an external field, an effective exchange field, an effective anisotropy field and a magnetostatic field. Some inter-diffusion usually occurs between the MR-enhancing Co layer and the NiFe layer adjacent to it [6]. In our simulations the NiFe/Co bilayer is replaced by a 8.1 nm composite layer with a bulk magnetization value $M_s = 848 \text{ kA/m}$ that is intermediate between the nominal bulk magnetization values of NiFe and Co, and chosen so that the contribution of each element is proportional to the thickness of its layer. Grain sizes of 25 nm in the plane of the film and thickness 8.1 nm, equal to the thickness of the layer, are used in the simulations. Each grain is

Contributions of the National Institute of Standards and Technology, not subject to copyright.

Manuscript received January 31, 1997.

J. O. Oti, 303-497-5557, fax 303-497-5316, oti@boulder.nist.gov; S. E. Russek, 303-497-5097, fax 303-497-5316, russek@boulder.nist.gov.

characterized by a local uniaxial magnetic anisotropy field of $H_k = 0.8$ kA/m in the longitudinal direction, and a maximum intergranular exchange field of 16 kA/m [7]. The exchange biasing of the pinned layer is simulated by superimposing a constant longitudinal field of 16 kA/m to the external field acting on the layer. The nonmagnetic copper layer is treated as free space in the calculations. The magnetoresistive change in resistance is calculated as $\Delta R/R = 1 - \cos\theta$, where θ is the angle between the average magnetization vectors of the layers. Self-field effects due to sense current in the device are neglected in the calculations.



(a)

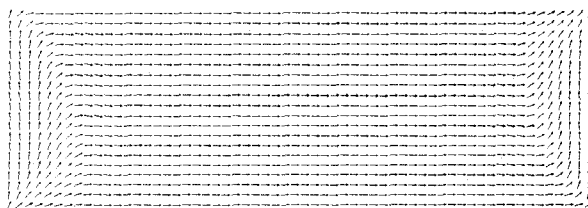
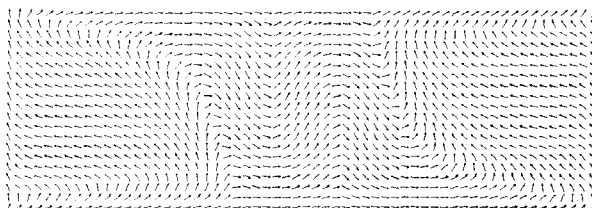
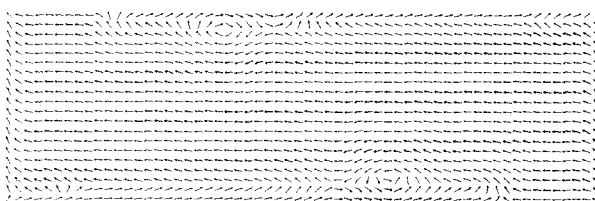
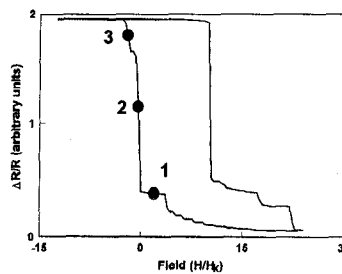
(b) $H_1 = 2H_k$ (c) $H_2 = -0.4H_k$ (d) $H_3 = -2H_k$

Fig. 2. Simulated switching sequence of a 3×1 μm MRAM spin valve: (a) MR curve of device. (b)-(d) Magnetization states of the free layer at different external fields. The arrows represent the projection in the film plane of the magnetization vectors of the grains. The magnetization of every other grain is skipped in the vector plots, to avoid clutter. The fields H_1 , H_2 and H_3 correspond to the points 1, 2 and 3 indicated on the MR curve.

Fig. 2 shows simulated vector plots of different stages of the magnetization reversal of the free layer of a 3×1 μm MRAM device having the MR curve shown in Fig 2(a). A magnetization of $.75M_s$ was used for this simulation. The lower branch of the

MR loop is traversed as the magnetic field is increased in opposition to the pinning field. The reversal process begins by the reversal at both ends of the sample, of spins that are nearer the center of the film edges (Fig 2(b)). As the negative field is increased, the two reversed central regions grow and approach each other. Demagnetizing effects inhibit the switching of the spins (Fig 2(c)) closer to the edges of the film. Fig. 2(d) shows a nearly completely reversed central domain region surrounded by narrow edge domains. The sizes of the edge domains depend primarily on the strength of the self-demagnetization of the film. The vortices formed near the film edges in Fig. 2(d) indicate the commencement of the reversal of the edge domains. A very large negative field is required to completely reverse the edge domains.

The magnetostatic interaction between the free and pinned layers and their self-demagnetization, have distinct effects on the shape of the MR curves. The interlayer coupling encourages the energetically favorable overall antiparallel orientation of magnetization vectors of the free and pinned layers. It therefore promotes the switching of the free layer into the antiparallel state but opposes its switching back into the parallel state. This accounts for the asymmetry about the origin, of the switching fields of the MR curve, defined as fields corresponding to $\Delta R/R = 1$. The self-demagnetization on the other hand opposes the switching of the free layer. In general, interlayer magnetostatic interaction effects are more pronounced



(a)

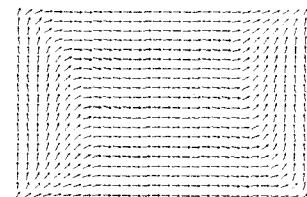
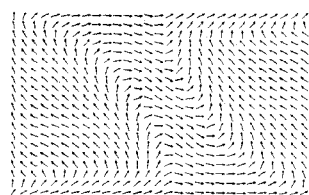
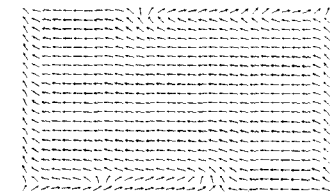
(b) $H_1 = 2H_k$ (c) $H_2 = -0.4H_k$ (d) $H_3 = -2H_k$

Fig. 3. Simulated switching sequence of a 1.5×1 μm MRAM spin valve: (a) MR curve of device. (b)-(d) Magnetization states of the free layer at different external fields. The arrows represent the projection in the film plane of the magnetization vectors of the grains. The fields H_1 , H_2 and H_3 correspond to the points 1, 2 and 3 indicated on the MR curve.

in smaller aspect ratio devices compared to larger aspect ratio devices. The negative switching fields of the devices decrease and the positive switching fields increase as the aspect ratio is decreased. The magnetization reversal of a 1.5×1 μm device is shown in Fig 3. The formation of the completely reversed

central region proceeds faster in this device than in the $3 \times 1 \mu\text{m}$ and the edge domains shown in the last panel are roughly of the same width as those in the $3 \times 1 \mu\text{m}$ device. The step-like structure in the branches in the MR curves are caused by Barkhausen jumps in the film that occur when individual single-domain regions in the sample switch abruptly.

Calculated MR curves of devices with different aspect ratios and a line width of $1 \mu\text{m}$ are shown in Fig. 4. An aspect ratio dependence similar to the one shown in the figure has been observed experimentally [8]. The 10:1 device shows an almost ideal MR behavior. Interlayer coupling effects are minimal for this device, and the self-demagnetization controls the switching of the free layer.

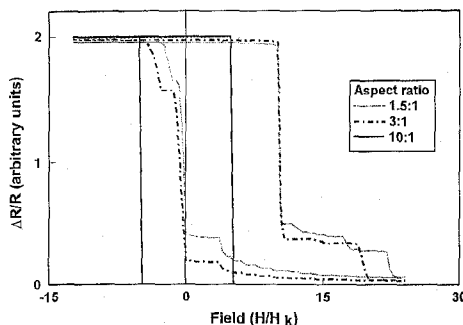


Fig. 4. Simulated MR curves of MRAM spin valves having a stripe height of $1 \mu\text{m}$, as a function of the aspect ratio of the device; $M = 0.75M_s$.

As pointed out previously, the magnetization of real films are reduced from their bulk values by interface effects, and the processing conditions they are subjected to during fabrication. The effect of the value of the magnetization of a film on the MR behavior of the device is illustrated in Fig. 5 in which are plotted the calculated MR curves of a $1.5 \times .5 \mu\text{m}$ device as a function of the magnetization of the magnetic layers. The magnetostatic coupling between the layers and their self-demagnetization increase as their magnetization increases. As the magnetization increases, the negative switching fields decrease and the positive switching fields increase because the interlayer magnetostatic coupling increases. At the maximum applied negative field, the magnetization state of the free layer resembles that shown in Fig. 3(d), with larger edge domains forming for larger magnetization values. The partially switched domain state is locked in place as the negative field is removed. The MR magnitude therefore decreases with increasing magnetization. For the device having $M = M_s$, if the negative field were increased further, the magnetization of the pinned layer would switch before the free layer is fully reversed. For a fixed aspect ratio and film thickness, magnetostatic effects increase as device line widths are made narrower. These effects, which were described above, are evident in Fig. 6, in which compare the MR curves of 1.5:1 devices with line widths 0.5 and $1.5 \mu\text{m}$.

III. CONCLUSIONS

The effects of the shape and sizes and magnetic properties of MRAM spin valves on their MR properties were studied using

a micromagnetics model. Magnetostatic effects increase in the samples as their magnetization are increased and as their aspect ratios decrease. The simulations suggest that interlayer magnetostatic interactions are primarily responsible for the observed asymmetries in MR curves. Devices with smaller aspect ratios display larger Barkhausen noises in their MR responses. Unswitched edge domains due to the self-demagnetization of the magnetic film, results in a decrease in the MR magnitude. These effects agree qualitatively with experimental measurements [8].

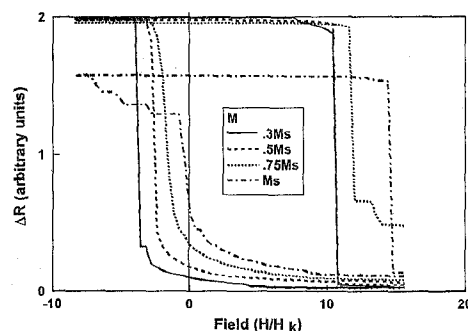


Fig. 5. Simulated MR curves of a $1.5 \times .5 \mu\text{m}$ MRAM spin valve as a function of the magnetization M of the magnetic layers; $M_s = 848 \text{ kA/m}$.

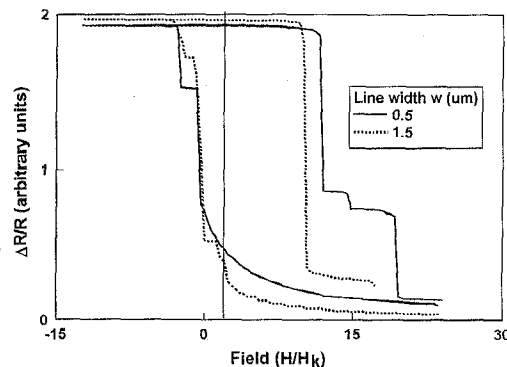


Fig. 6. Simulated MR curves of a 1.5:1 MRAM spin valve as a function of line width w ; $M = 0.75M_s$.

REFERENCES

- [1] D. D. Tang, P. K. Wang, V. S. Speriosu, S. Le and K. K. Kung, "Spin-valve RAM cell," *IEEE Trans. Magn.*, vol. 31, 3206 (1995).
- [2] A. V. Pohm, J. S. T. Huang, J. M. Daughton, D. R. Krahn and V. Mehra, "The design of a one megabit nonvolatile M-R memory chip using $1.5 \times 1.5 \text{ nm}$ cells," *IEEE Trans. Magn.*, vol. 24, 3117 (1988).
- [3] J. M. Daughton, "Magnetic tunneling applied to memory," paper AA-04, 41st MMM Conference, Atlanta, Georgia, Nov. 1996.
- [4] Y. Zheng and J-G. Zhu, "Micromagnetics of spin valve memory cell," *IEEE Trans. Magn.* vol. 32, 4237 (1996).
- [5] B. A. Everitt, A. V. Pohm and J. M. Daughton, "Size dependence of switching thresholds for pseudo spin valve MRAM cells," *J. Appl. Phys.*, vol. 81 (8), 4020 (1997).
- [6] S. S. P. Parkin, "Dramatic enhancement of interlayer exchange coupling and giant magnetoresistance in $\text{Ni}_3\text{Fe}/\text{Cu}$ multilayers by addition of thin Co interface layers," *Appl. Phys. Lett.*, vol. 61, 1358 (1992).
- [7] J. O. Oti, "A micromagnetic model of dual-layer magnetic recording thin films," *IEEE Trans. Magn.*, vol. 29, 1265 (1993).
- [8] S. E. Russek, J. O. Oti, Y. K. Kim and R. W. Cross, "Performance optimization of submicrometer spin valves for digital applications," these proceedings.